

# A Recently Revived and Produced Global Air-sea Surface Turbulent Fluxes Dataset -- GSSTF2b: Validations and Findings

Chung-Lin Shie<sup>1,2</sup>, Long S. Chiu<sup>3,4</sup>, Robert Adler<sup>2,5</sup>, Si Gao<sup>4</sup>, R. Chokngamwong<sup>4</sup>, I-I Lin<sup>6</sup>, Eric Nelkin<sup>2,7</sup>, Joe Ardizzone<sup>8</sup>, Pingping Xie<sup>9</sup>, and Feng-Chin Wang<sup>10</sup>

<sup>1</sup>UMBC/GEST, Baltimore, Maryland, USA

<sup>2</sup>Code 613.1, NASA/GSFC, Greenbelt, Maryland, USA ([Chung-Lin.Shie-1@nasa.gov](mailto:Chung-Lin.Shie-1@nasa.gov))

<sup>3</sup>GMU/CEOSR, Fairfax, Virginia, USA

<sup>4</sup>CUHK/ISEIS, Shatin NT, Hong Kong, China

<sup>5</sup>UMCP/ESSIC, College Park, Maryland, USA

<sup>6</sup>NTU, Taipei, Taiwan

<sup>7</sup>SSAI, Lanham, Maryland, USA

<sup>8</sup>SAIC, Greenbelt, Maryland, USA

<sup>9</sup>NOAA/CPC, Camp Springs, Maryland, USA

<sup>10</sup>CWB, Taipei, Taiwan

## Abstract

Accurate sea surface flux measurements are crucial to understanding the global water and energy cycles. Remote sensing is a valuable tool for global monitoring of these flux measurements. The GSSTF (Goddard Satellite-based Surface Turbulent Fluxes) algorithm was thus developed and applied to remote sensing research and applications. The subsequently produced daily global ( $1^\circ \times 1^\circ$ ) GSSTF2 (Version-2) dataset (July 1987-December 2000) has been widely used by the scientific community for global energy and water cycle research, as well as regional and short period data analyses since its official release in 2001.

We have recently been funded by the NASA/MEaSUREs Program to resume processing of the GSSTF with an objective of continually producing an up-to-date uniform and reliable dataset of sea surface turbulent fluxes, derived from improved input remote sensing data and model reanalysis, which would continue to be useful for global energy and water flux research and applications. The daily global ( $1^\circ \times 1^\circ$ ) GSSTF2b (Version-2b) dataset (July 1987-December 2008) has lately been produced using upgraded and improved input datasets such as the Special Sensor Microwave Imager (SSM/I) Version-6 (V6) product (including brightness temperature [ $Tb$ ], total precipitable water [ $W$ ], and wind speed [ $U$ ]) and the NCEP/DOE Reanalysis-2 (R2) product (including sea skin temperature [ $SKT$ ], 2-meter air temperature [ $T2m$ ], and sea level pressure [ $SLP$ ]). The input datasets previously used for producing the GSSTF2 product were the SSM/I Version-4 (V4) product and the NCEP Reanalysis-1 (R1) product. The newly produced GSSTF2b turbulent fluxes, along with their counterparts from GSSTF2, have been validated using available sounding observations obtained from five field experiments. The GSSTF2b product has been found to generally agree better with the sounding observations than its counterpart (GSSTF2) does in all three flux components – latent heat flux ( $LHF$ ), sensible heat flux ( $SHF$ ), and wind stress ( $WST$ ). The major meteorological input variables such as wind speed, total & bottom-layer precipitable water ( $W$  &  $WB$ ), and surface air & sea humidity ( $Qa$  &  $Qs$ ) of GSSTF2b and GSSTF2 have also been examined and compared, along with the three flux components, for global and regional scales in this study. The SSM/I  $Tb$  (i.e.,  $Tb19v$  and  $Tb22v$ ), which was used to retrieve  $WB$  and thus  $Qa$ , was found to indirectly carry out a critical impact on the global tendency/trend found in our GSSTF  $LHF$  products. This crucial finding, however, won't be discussed in this extended abstract due to a page-limit requirement.

Key word: Air-sea turbulent fluxes, global, satellite-based

## 1. Introduction

The Earth's climate is characterized by innumerable processes that couple the atmosphere, ocean and land systems. The global water cycle's provision of water to terrestrial storage, reservoirs, and rivers hinges on the global excess of evaporation to precipitation over the oceans. This ocean evaporation excess would vary and ultimately lead to variations in the amount of freshwater that is transported and precipitated

over continental regions. The air-sea fluxes of momentum, radiation and freshwater (precipitation – evaporation) play a very crucial role in a wide variety of atmospheric and oceanic problems. Information on these fluxes is important in understanding the air-sea interaction, global energy and water cycle variability, and in improving model simulations of climate variations. These fluxes are thus required for driving ocean models and validating coupled ocean–atmosphere global models. Surface measurements of these fluxes are scarce in both

space and time, especially over the oceans and in remote land areas. The SSM/I on board a series of Defense Meteorological Satellite Program (DMSP) satellites spacecraft has provided global radiance measurements for sensing the atmosphere and the surface. The GSSTF algorithm was thus developed and applied to remote sensing research and applications. The subsequently produced daily global ( $1^\circ \times 1^\circ$ ) GSSTF2 (Version-2) dataset (July 1987-December 2000) has been widely used by the scientific community for global energy and water cycle research, as well as regional and short period data analyses since its official release in 2001 by NASA/GSFC Data Information Service Center (DISC). However, the GSSTF2 production project ended during 2001. We have recently been funded (starting May 2008) by the NASA/ MEaSUREs [Making Earth System data records for Use in Research Environments] Program to resume processing of the GSSTF with an objective of continually producing up-to-date uniform and reliable datasets of sea surface turbulent fluxes, derived from improved input remote sensing data and model reanalysis, which would continue to be useful for global energy and water flux research and applications (Shie et al. 2009). The proposed GSSTF production consists of two phases: (1) reprocessing/extension of the  $1^\circ \times 1^\circ$  (latitude-longitude) GSSTF2b (Version-2b, first-phase) datasets over global oceans for a 21.5-yr of period from July 1987 to Dec 2008 using the improved SSM/I V6 (Wentz/RSS) surface wind, total precipitable water and microwave brightness temperature data, as well as the recently released NCEP/DOE Reanalysis-2 (R2) sea surface skin temperature, 2-meter air temperature, and sea level pressure and (2) production of a further improved GSSTF3 (Version-3, second-phase) dataset with a finer spatial resolution ( $0.25^\circ \times 0.25^\circ$  latitude-longitude) using the sea surface temperature from AMSR-E and TMI, and ocean surface wind vector from QuikSCAT and ADEOS2-SeaWinds, over the global oceans for the period July 1999–Dec 2009.

The first-phase product, i.e., daily global ( $1^\circ \times 1^\circ$ ) GSSTF2b dataset (July 1987-December 2008) has lately been completed using the aforementioned upgraded and improved input datasets such as the SSM/I V6 product and the NCEP/DOE R2 product. The input datasets previously used for producing the GSSTF2 product were the SSM/I V4 product and the NCEP R1 product. GSSTF2b will soon be officially released by NASA GES (Goddard Earth Science) DISC (Shie et al. 2010). The production of GSSTF3b is currently in processing.

The bulk flux model used for producing the GSSTF2b is described in section 2. Results and discussions are presented in section 3 followed by an acknowledgement in section 4.

## 2. The bulk flux model

The bulk flux model (based on the surface layer

similarity theory, Chou 1993) used for producing the GSSTF2b fluxes is essentially the same as that for GSSTF2 (Chou et al. 2003). Similar to GSSTF2, GSSTF2b requires the same methodology and same kinds of input data such as the SSM/I surface/10-m wind speeds, total precipitable water, bottom-layer (500 m) precipitable water, and the NCEP-NCAR reanalysis of sea surface skin temperature, 2-m air temperature, and sea level pressure.

The air-sea turbulent fluxes, i.e., wind stress ( $\tau$ ), sensible heat flux ( $SHF$ ), and latent heat flux ( $LHF$ ) can be given in the following bulk aerodynamic formula:

$$\tau = \rho C_D (U - U_s)^2, \quad (1a)$$

$$SHF = \rho C_p C_H (U - U_s) (\theta_s - \theta_a), \quad (1b)$$

$$LHF = \rho L_v C_E (U - U_s) (Q_s - Q_a), \quad (1c)$$

where  $\rho$  is air density,  $C_p$  the isobaric specific heat,  $L_v$  the latent heat of vaporization,  $C_D$ ,  $C_H$ ,  $C_E$  the three respective bulk transfer coefficients, and  $U_s$  is the negligibly small ocean surface current (about 0.55 of frictional velocity). The input parameters are the wind speed ( $U$ ), the sea surface temperature ( $\theta_s$ ), the air potential temperature ( $\theta_a$ ), the specific humidity ( $Q_a$ ) at the reference height, and the saturation specific humidity ( $Q_s$ ) at the sea surface temperature.

Based on surface layer similarity theory, the surface fluxes in Eqs. (1a)-(1c) can also be derived from the scaling parameters for wind or friction velocity ( $u^*$ ), temperature ( $\theta^*$ ), and humidity ( $q^*$ ) as

$$\tau = \rho u^{*2}, \quad (2a)$$

$$SHF = -\rho C_p u^* \theta^*, \quad (2b)$$

$$LHF = -\rho L_v u^* q^* \quad (2c)$$

For a given  $\theta_s$  (or  $SKT$ ) and wind, temperature, and humidity at the measurement or reference heights within the atmospheric surface layer, the scaling parameters are solved through the roughness lengths and dimensionless gradients of wind, temperature, and humidity. The dimensionless gradients of wind, potential temperature, and humidity are functions of the stability parameter  $z/L$ , where  $z$  is the measurement height, and  $L$  the Monin-Obukhov length, which depends on the scaling parameters or fluxes (detailed description can be found in Chou et al. 2003). Accordingly, the transfer coefficients, which reflect the efficiency of the vertical transportation of momentum, heat, and moisture flux, are a non-linear function of the vertical gradient in wind speed, temperature and water vapor near the surface and, therefore, are affected by the stability of the surface air. Liu et al. (1979) performed detailed analysis of the transfer coefficients based on their model and predicted that under low wind conditions the transfer coefficient might increase with increasing wind speed, because the increased roughness facilitates the transfer of heat and vapor. However, as the wind speed increases further,

the sheltering effect due to the troughs between waves becomes more significant and will suppress the exchange of vapor and heat. As the wind speed reaches about  $5 \text{ m s}^{-1}$ , the negative and positive effects due to increased wind speed counterbalance each other. If wind speed increases further, the transfer coefficient may even start to decrease. Latest field and laboratory measurements have shown that the drag coefficient does not increase with wind speed at extreme wind conditions, i.e., greater than  $30 \text{ m s}^{-1}$ . Therefore, high-wind transfer coefficients may be applied for the 10-m winds beyond  $18 \text{ m s}^{-1}$  (or even higher) for our future production of GSSTF3. Such a high-wind treatment may improve the surface flux retrieval, as well as provide a better understanding of weather systems with high winds such as tropical cyclones, hurricanes and typhoons. The implementation of high wind coefficient treatment to the bulk flux model is currently still under developing and testing. The GSSTF2b turbulent fluxes presented in this study are produced still using the same model set-up for producing GSSTF2.

### 3. Results and discussions

The SSM/I V4 surface wind speeds used for the GSSTF2 production was found carrying a linear trend of 6% increase in a 13.5-year period (Xing 2006). Wentz of RSS removed such spurious trends in the latest issued SSM/I V6 product. Shie et al. (2009) recently showed a consistent improvement in the surface wind speed from SSM/I V4 to V6 by comparing the respective daily V6 and V4 (combined F13 and F14) surface wind speeds of a 46-day period (i.e., 28 July - 11 September 1999) with the corresponding Kwajalein Experiment (KWAJEX) in situ observed wind speeds. Statistics indicated a rising correlation coefficient from 0.84 (V4) to 0.89 (V6), a significant reduction of root-mean-square (RMS)/stand-deviation-error (SDE) from 0.90/0.90 (V4) to 0.69/0.79  $\text{m s}^{-1}$  (V6), and an improved bias reduced from 0.15 (V4) to 0.10  $\text{m s}^{-1}$  (V6). SDE is the standard deviation of the differences between the computed and observed. An extended validation on the SSM/I surface wind speed has been further conducted by including four more field experiments. Table 1 shows the periods and locations of these five 1999 experiments, i.e., KWAJEX, the Joint Air–Sea Monsoon Interaction Experiment (JASMINE), the buoy service in the North Pacific (MOORINGS), the Nauru’99 (NAURU99), and the Pan–American Climate Study in the eastern Pacific during 1999 (PACSF99). Like an earlier finding from KWAJEX (Shie et al. 2009), SSM/I wind speeds are also found improved (i.e., closer to the observed) from V4 to V6 for JASMINE, MOORINGS, and PACSF99. Statistics show a commonly reduced RMS, SDE, and bias for these three experiments, while correlation coefficient increases by a considerable amount of 0.11 (i.e., from 0.77/V4 to 0.88/V6) for MOORINGS. However, the V6 wind speed performs poorly for NAURU with even a negative correlation coefficient that costly turns around an otherwise overall better

performance in V6. Figure 1 shows the associated daily SSM/I V6 (shown in red dot) and V4 (shown in blue dot) wind speeds compared to their observed counterparts (all five experiments combined), respectively. For those V6 sample data that are relatively far away from (and parallel to) the dark diagonal line (Fig. 1) are mostly contributed by NAURU. The supposedly trend-removed V6 wind speeds seemingly cannot guarantee a common improvement among all the five experiments.

The SSM/I  $W$  and  $W_B$  that are used to retrieve  $Qa$  using an EOF method (Chou et al. 1995) are, however, found varied insignificantly from V4 to V6, unlike what has been shown in surface wind speed (Fig. 1). The daily  $W$  of SSM/I V6 vs V4 (combined F13 and F14; collected by collocating with the same set of sample observations consisting of the five field experiments) has a very close distribution with a correlation of 0.999, while V6 is slightly larger than V4 with a positive bias of  $0.22 \text{ g kg}^{-1}$  relative to a V4 mean of  $45.36 \text{ g kg}^{-1}$  (not shown). Like  $W$ , the associated daily  $W_B$  of V6 vs V4 shown in Fig. 2 demonstrates a similar and consistent feature (with a correlation of 0.996) that V6 is slightly larger than V4 with a positive bias of  $0.015 \text{ g kg}^{-1}$  relative to a V4 mean of  $0.995 \text{ g kg}^{-1}$ . However, the upgrading from V4 to V6 might have caused a slightly greater impact on  $W_B$  than  $W$  based on the magnitude of a ratio of the bias (difference between V6 and V4) to the V4 mean. Accordingly,  $W_B$  has a ratio of 1.51% ( $0.015/0.995$ ) that is greater than 0.49% ( $0.22/45.36$ ) of  $W$ .

The daily  $Qa$  retrieved based on  $W$  and  $W_B$  from the respective SSM/I V6 and V4 are shown in Fig. 3 vs the observed  $Qa$  from the five experiments altogether. The retrieved humidity using the upgraded V6 is found with a slightly improved correlation (0.86) and yet a higher bias ( $0.82 \text{ g kg}^{-1}$ ) than those of V4 ( $0.85$  and  $0.59 \text{ g kg}^{-1}$ , respectively). The quantitative (ratio) analysis applied for  $W$  and  $W_B$  is also performed for  $Qa$ . The ratio of the increased bias in  $Qa$  ( $0.23 \text{ g kg}^{-1}$ , i.e., from  $0.59 \text{ g kg}^{-1}$  of V4 to  $0.82 \text{ g kg}^{-1}$  of V6) to the mean  $Qa$  of V4 ( $18.25 \text{ g kg}^{-1}$ ) is 1.26%, which is considerably closer to that of  $W_B$  (1.51 %) than that of  $W$  (0.49 %). It further confirms that the retrieved specific humidity highly depends on the water vapor in the lower part of PBL, i.e.,  $W_B$ .

Finally, the newly produced GSSTF2b fluxes, i.e.,  $LHF$ ,  $SHF$  and  $WST$ , along with their counterparts from GSSTF2, have been validated against the ship measurements from the aforementioned five 1999 experiments (Figs 4-6). It is found that the GSSTF2b product generally agrees better with the observations than its counterpart (GSSTF2) does in all three flux components. All three flux quantities of GSSTF2b are found with a higher/better correlation than those of GSSTF2. Note that "GO" (in green) represents the fluxes produced by directly applying the observational

input parameters into the GSSTF model. As expected, "GO" possesses the best statistics (compared to both V6 and V4) that first ensures us a fine and physical-consistent GSSTF model. It also implies that there is always room for us to thrive for improving our retrieval scheme, as well as acquiring more realistic and reliable input datasets/parameters.

#### 4. Acknowledgement

The first author would like to dedicate this paper on the GSSTF2b product to his mentor: the late research scientist S.-H. Chou (aka Sue). Without her genuine intelligence, intuition, great vision, and perseverance, the productions of GSSTF1 and GSSTF2, and now GSSTF2b would have not been possible. This study is supported by the MEaSUREs Program of NASA Science Mission Directorate-Earth Science Division. The first author is especially grateful to its Program Manager M. Maiden for her support of this research. The first author would also like to thank Renguang Wu and Kyle Hilburn for their precious helps during our GSSTF2b production.

#### 5. References

Chou, S.-H., 1993: A comparison of airborne eddy correlation and bulk aerodynamic methods for ocean-air turbulent fluxes during cold-air outbreaks. *Bound.-Layer Meteor.*, **64**, 75–100.

Chou, S.-H., R. M. Atlas, C-L. Shie and J. Ardizzone, 1995: Estimates of surface humidity and latent heat fluxes over oceans from SSM/I data, *Monthly Weather Review*, **123**, 2405–2425.

Chou, S.-H., E. Nelkin, J. Ardizzone, R. M. Atlas, and C-L. Shie, 2003: Surface turbulent heat and momentum fluxes over global oceans based on the Goddard satellite retrieval, version 2 (GSSTF2). *J. Climate*, **16**, 3256–3273.

Liu, W. T., K. B. Katsaros, and J. A. Businger, 1979: Bulk parameterization of air-sea exchanges of heat and water vapor including the molecular constraints at the interface. *J. Atmos. Sci.*, **36**, 1722–1735.

Shie, C.-L., L. S. Chiu, R. Adler, P. Xie, I-I Lin, F.-C. Wang, E. Nelkin, R. Chokngamwong, W. S. Olson, and D. A. Chu, 2009: A note on reviving the Goddard Satellite-based Surface Turbulent Fluxes (GSSTF) dataset, *Advances in Atmospheric Sciences*, **Vol. 26**, No. 6, 1071–1080.

Shie, C.-L., and collaborators, 2010: The Goddard Satellite-Based Surface Turbulent Fluxes Dataset --- Version 2b (GSSTF 2b) [global (grid of 1°x1°) daily air-sea surface fluxes from July 1987 to December 2008] distributed by *Goddard DAAC* in spring 2010.

Xing, Yukun, 2006: Recent changes in oceanic latent

heat flux from remote sensing, Ph.D. Dissertation, School of Computational Science, George Mason University, Fairfax VA 22030, 119 pp.

**Table 1.** Times and locations of five 1999 field experiments conducted by the NOAA/ETL research ships.

Field Experiments	Times	Locations
JASMINE	4–31 May 99	5°S–13°N, 88°–98°E
KWAJEX	28 Jul–10 Sep 99	9°N, 167°E
MOORINGS	14 Sep–21 Oct 99	8°N, 167°E–49°N, 130°W
NAURU99	15 Jun–18 Jul 99	12°S, 130°E–8°N, 167°E
PACSF99	2 Nov–1 Dec 99	8°S–12°N, 95°–121°W

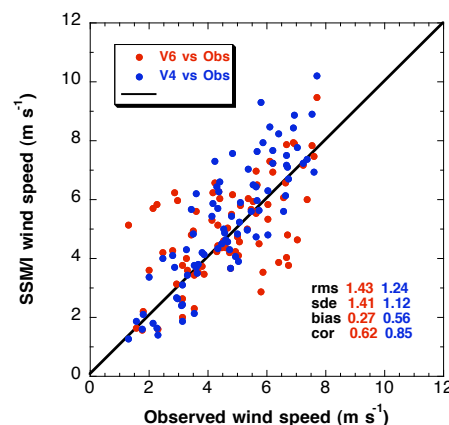


**Figure 1:** The respective Wentz Version 6 (red solid circle) and Version 4 (blue solid triangle) (combined F13 and F14) daily surface wind speed vs the observed from the five experiments altogether.

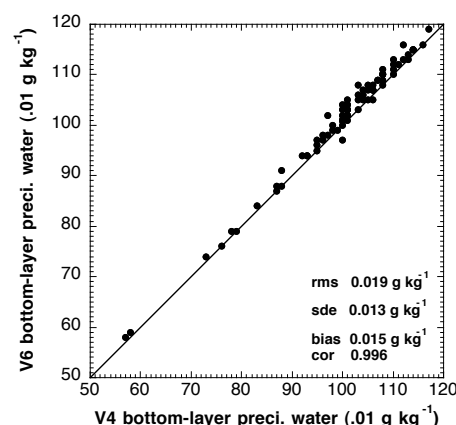


**Figure 2:** Bottom-layer precipitable water retrieved from SSM/I Version 6 vs that from Version 4 based on the sample data collocated with the five experiments.

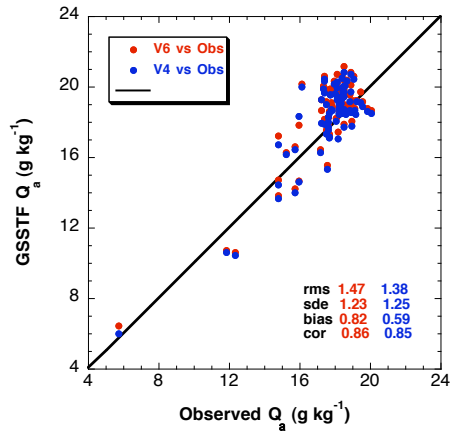


**Figure 3:** The respective Wentz Version 6 (red solid circle) and Version 4 (blue solid triangle) (combined F13 and F14) daily surface air humidity vs the observed from the five experiments altogether.

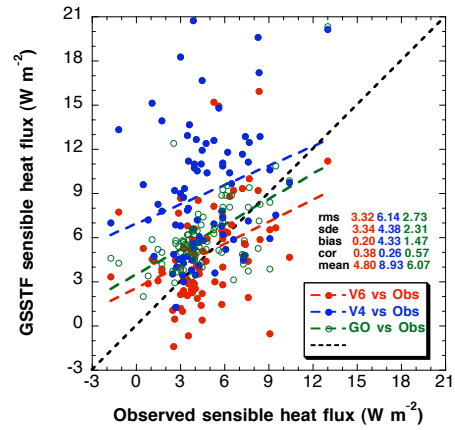


**Figure 5:** The respective Wentz Version 6 (red solid circle) and Version 4 (blue solid triangle) (combined F13 and F14) daily sensible heat flux vs the observed from the five experiments altogether. The daily sensible heat flux (“GO”) computed by applying ship data into the GSSTF2 bulk flux model vs the observed is also shown (green open circle).

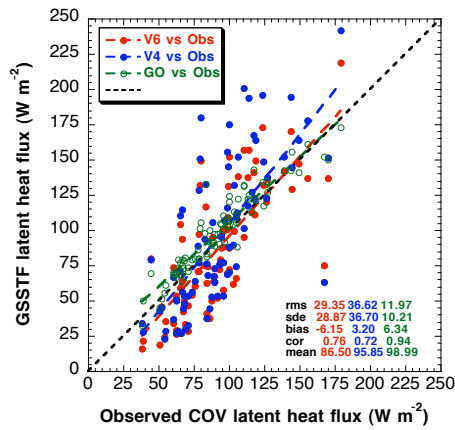


**Figure 4:** The respective GSSTF2b (based on combined F13 and F14 of V6) (red solid circle) and GSSTF2 (based on combined F13 and F14 of V4) (blue solid triangle) daily latent heat flux vs the observed from the five experiments altogether. The daily latent heat flux (“GO”) computed by applying ship data into the GSSTF2 bulk flux model vs the observed is also shown (green open circle).

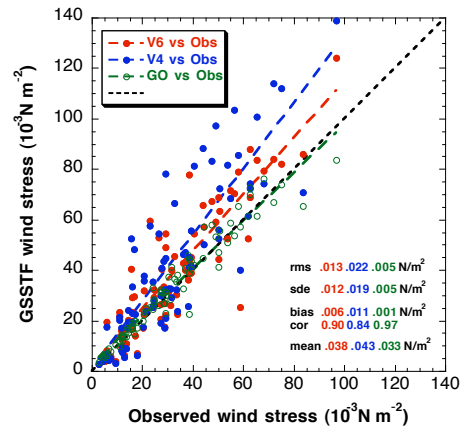


**Figure 6:** The respective Wentz Version 6 (red solid circle) and Version 4 (blue solid triangle) (combined F13 and F14) daily wind stress vs the observed from the five experiments altogether. The daily wind stress (“GO”) computed by applying ship data into the GSSTF2 bulk flux model vs the observed is also shown (green open circle).

